Inorganic Chemistry
Article

Inorg. Chem. **2009**, *48*, 5195–5207 **5195**
DOI: 10.1021/ic9001175

Binuclear Cobalt Complexes of Schiff-Base Calixpyrroles and Their Roles in the Catalytic Reduction of Dioxygen

Manuel Volpe,[†] Heather Hartnett,[‡] James W. Leeland,[†,‡] Kathryn Wills,[†] Marianne Ogunshun,[†] Bridgette J. Duncombe,[†] Claire Wilson,[‡,§] Alexander J. Blake,[‡] Jon McMaster,[‡] and Jason B. Love*[,†]

[†]*EaStCHEM School of Chemistry, University of Edinburgh, The King's Buildings, West Mains Road, Edinburgh EH9 3JJ, United Kingdom,* [‡]*School of Chemistry, University of Nottingham, University Park, Nottingham NH7 2RD, United Kingdom, and* [§]*Rigaku Europe, Chaucer Business Park, Watery Lane, Sevenoaks, Kent TN15 6QY, United Kingdom*

Received January 20, 2009

The syntheses and characterization of a series of binuclear cobalt complexes of the octadentate Schiff-base calixpyrrole ligand L are described. The cobalt(II) complex $[Co_2(L)]$ was prepared by a transamination method and was found to adopt a wedged, Pac-man geometry in the solid state and in solution. Exposure of this compound to dioxygen resulted in the formation of a 90:10 mixture of the peroxo $[Co_2(O_2)(L)]$ and superoxo $[Co_2(O_2)(L)]^+$ complexes in which the peroxo ligand was found to bind in a Pauling mode in the binuclear cleft in pyridine and acetonitrile adducts in the solid state. The dioxygen compounds can also be prepared directly from $Co(OAc)_2$ and H_4L under aerobic conditions in the presence of a base. The reduction of dioxygen catalyzed by this mixture of compounds was investigated using cyclic voltammetry and rotating ring disk electrochemistry and, in acidified ferrocene solutions, using UV−vis spectrophotometry, and although no formation of peroxide was seen, reaction rates were slow and had limited turnover. The deactivation of the catalyst material is thought to be due to a combination of the formation of stable hydroxy-bridged binuclear complexes, for example, $[Co_2(OH)(L)]^+$, an example of which was characterized structurally, and the catalytic resting point, the superoxo cation, is formed by a pathway independent of the major peroxo product. Collision-induced dissociation mass spectrometry experiments showed that, while $[Co_2(O_2)(L)]H^+$ ions readily lose a single O atom, the resulting Co−O(H)−Co core remains resistant to further fragmentation. Furthermore, DFT calculations show that the O−O bond distance in the dioxygen complexes is not a good indicator of the degree of reduction of the O_2 unit and provide a reduction potential of ca. +0.40 V versus the normal hydrogen electrode for the $[Co_2(O_2)(L)]^{+/0}$ couple in dichloromethane solution.

Introduction

The oxygen reduction reaction (ORR) to water is a chemical redox reaction that is fundamental to the fuel cell technologies that underpin a low-carbon, hydrogen-based economy.[1] In a polymer electrolyte fuel cell, a potential power source for zero-emission vehicles, this reaction is currently catalyzed at platinum metal-based electrodes. However, the high cost of this precious metal and the high loading required for the electrode to function appropriately, the need for overpotentials to be applied, and the problems associated with electrode poisoning and degradation necessitate the development and exploitation of new, nonprecious-metal catalysts to fully enable this technology.[2,3]

The most promising class of nonprecious-metal oxygen reduction catalysts are derived from iron and cobalt complexes of N-donor ligands such as porphyrins, phthalocyanines, and aza-macrocycles and also from more simple combinations of metal, nitrogen, and carbon sources. While materials derived directly from these metal complexes generally have limited use as ORR catalysts, pyrolysis at temperatures between 400 and 1000 °C results in materials containing $M-N_x$ surface species that can act as very active catalysts and that display similar characteristics to those of platinum.[3] More recently, however, it was shown that a composite of cobalt cations and polypyrrole on a carbon support forms a cathodic electrode material that displays activity similar to that of platinum-based electrodes and remarkable stability.[4] Significantly, and unlike materials derived from MN_4 complexes, no sintering of this electrode was required to provide appreciable activity. Even so, surface analysis of this material by XANES and XAFS suggests that cobalt(II) cations are present at the

*To whom correspondence should be addressed. Tel.: +44 131 6504762. E-mail: jason.love@ed.ac.uk.

(1) (a) Adler, S. B. *Chem. Rev.* **2004**, *104*, 4791. (b) Lewis, N. S.; Nocera, D. G. *Proc. Natl. Acad. Sci. U.S.A.* **2006**, *103*, 15729. (c) Dempsey, J. L.; Esswein, A. J.; Manke, D. R.; Rosenthal, J.; Soper, J. D.; Nocera, D. G. *Inorg. Chem.* **2005**, *44*, 6879.

(2) (a) Alonso-Vante, N.; Feng, Y. *Phys. Status Solidi B* **2008**, *245*, 1792. (b) Matter, P. H.; Biddinger, E. J.; Ozkan, U. S. *Catalysis* **2007**, *20*, 338. (c) Wang, B. *J. Power Sources* **2005**, *152*, 1.

(3) Bezerra, C. W. B.; Zhang, L.; Lee, K.; Liu, H.; Marques, A. L. B.; Marques, E. P.; Wang, H.; Zhang, J. *Electrochim. Acta* **2008**, *53*(15), 4937.

(4) Bashyam, R.; Zelenay, P. *Nature* **2006**, *443*, 63.

Published on Web 05/11/2009

Chart 1. Comparison between Pac-man Diporphyrin and Schiff-Base Calixpyrrole Complexes

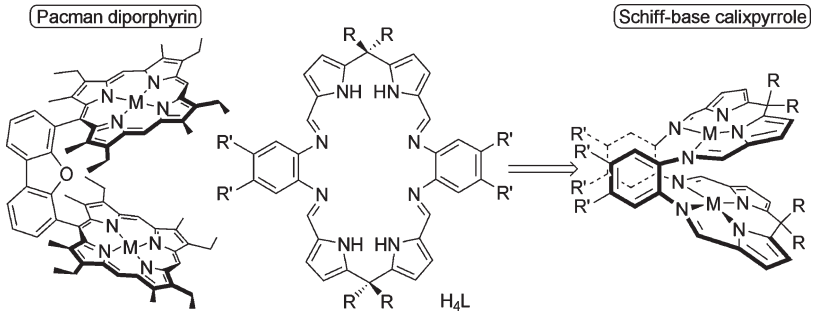

electrode surface and that they are stabilized by coordinative bonding to N or O.

While the most promising nonplatinum electrode materials to date have been developed using high-temperature sintering or supported-metal methods, many of the fundamental mechanistic aspects of dioxygen reduction catalysis have been elucidated by extensive research into molecular transition metal dioxygen complexes. In particular, binuclear cobalt compounds of cofacial diporphyrins have been shown to manage successfully the multiple proton-coupled electron-transfer (PCET) chemistry that operates during the four-electron reduction of dioxygen to water, as opposed to the two-electron routes normally seen using mononuclear porphyrin complexes.[5,6] This chemistry benefits from the use of prefabricated ligands, in this case, cofacial diporphyrins, which control precisely the primary coordination spheres and the relative positioning of the two metals, and enables tuning of the reaction attributes through subtle modification of the ligand environment. For example, ligand modifications to form binucleating porphyrin−corrole, corrole−corrole, and porphyrin−"hangman" ligands with rigid single-pillar backbones results in metal complexes that exhibit relevant PCET chemistry and that can act as ORR catalysts.[7,8]

As an alternative approach, we,[9,10] and Sessler and co-workers,[11] have shown that mono- and binuclear complexes of the Schiff-base calixpyrrole macrocycles H_4L (Chart 1) adopt rigid wedged structures that are reminiscent of those of cofacial, or Pac-man, diporphyrins, albeit with much more geometrically constrained architectures. Importantly, and in contrast to the porphyrinic analogues, these macrocyclic ligands are prepared straightforwardly in a modular manner, in high yield, and on a large scale (> 30 g) from inexpensive starting materials (pyrrole, ketone, and aromatic diamine).

Significantly, we described in a recent communication that the binuclear cobalt complex $[Co_2(L)]$ (R = Me, R′ = H) reacts with dioxygen to form a 90:10 mixture of peroxo $[Co_2(O_2)(L)]$ and superoxo complexes $[Co_2(O_2)(L)]^+$.[12] The peroxo was found to bridge the two cobalt(III) centers in a zigzag, Pauling bonding mode in the solid state and, so, provides some insight into the dioxygen reduction chemistry exhibited by related binuclear cobalt complexes of cofacial diporphyrins. In the case of the latter porphyrinic compounds, the resting state of the catalytic reduction reaction is the superoxo cation $[Co_2(O_2)(diporph)]^+$ (where diporph is a cofacial or Pac-man diporphyrin ligand), in which the superoxo ligand has been shown by calculation to adopt either Griffith or Pauling bonding geometries between the two metals.[13,14] In this contribution, we expand on our recently communicated dioxygen chemistry of $[Co_2(L)]$, in particular by assessing these materials as catalysts for dioxygen reduction and presenting some insight into possible pitfalls in the catalytic process that operates using these catalysts.

Experimental Section

Air-sensitive metal complexation reactions were carried out using standard Schlenk line techniques or in a Vacuum Atmospheres OmniLab glovebox. The compounds H_4L and $[Co(thf)\{N(SiMe_3)_2\}_2]$ were prepared using literature procedures.[10,15] THF and toluene were dried by passage through columns of activated alumina and collection under an inert atmosphere, while benzonitrile was dried over CaH_2 and trap-to-trap distilled. Deuteriated solvents were

(5) (a) Rosenthal, J.; Nocera, D. G. *Prog. Inorg. Chem.* **2007**, *55*, 483. (b) Collman, J. P.; Wagenknecht, P. S.; Hutchinson, J. E. *Angew. Chem., Int. Ed.* **1994**, *33*, 1537.

(6) Rosenthal, J.; Nocera, D. G. *Acc. Chem. Res.* **2007**, *40*, 543.

(7) (a) Kadish, K. M.; Shen, J.; Fremond, L.; Chen, P.; El Ojaimi, M.; Chkounda, M.; Gros, C. P.; Barbe, J.-M.; Ohkubo, K.; Fukuzumi, S.; Guilard, R. *Inorg. Chem.* **2008**, *47*(15), 6726. (b) Kadish, K. M.; Fremond, L.; Burdet, F.; Barbe, J.-M.; Gros, C. P.; Guilard, R. *J. Inorg. Biochem.* **2006**, *100*(4), 858. (c) Kadish, K. M.; Shao, J.; Ou, Z.; Fremond, L.; Zhan, R.; Burdet, F.; Barbe, J.-M.; Gros, C. P.; Guilard, R. *Inorg. Chem.* **2005**, *44*(19), 6744. (d) Rosenthal, J.; Chng, L. L.; Fried, S. D.; Nocera, D. G. *Chem. Commun.* **2007**, *25*, 2642. (e) Soper, J. D.; Kryatov, S. V.; Rybak-Akimova, E. V.; Nocera, D. G. *J. Am. Chem. Soc.* **2007**, *129*(16), 5069. (f) Liu, S.-Y.; Nocera, D. G. *J. Am. Chem. Soc.* **2005**, *127*, 5278. (g) Chng, L. L.; Chang, C. J.; Nocera, D. G. *Org. Lett.* **2003**, *5*(14), 2421. (h) Yeh, C.-Y.; Chang, C. J.; Nocera, D. G. *J. Am. Chem. Soc.* **2001**, *123*(7), 1513.

(8) Kadish, K. M.; Fremond, L.; Ou, Z.; Shao, J.; Shi, C.; Anson, F. C.; Burdet, F.; Gros, C. P.; Barbe, J.-M.; Guilard, R. *J. Am. Chem. Soc.* **2005**, *127*(15), 5625.

(9) (a) Givaja, G.; Blake, A. J.; Wilson, C.; Schröder, M.; Love, J. B. *Chem. Commun.* **2003**, 2508. (b) Arnold, P. L.; Patel, D.; Blake, A. J.; Wilson, C.; Love, J. B. *J. Am. Chem. Soc.* **2006**, *128*, 9610. (c) Arnold, P. L.; Patel, D.; Wilson, C.; Love, J. B. *Nature* **2008**, *451*, 315. (d) Volpe, M.; Reid, S. D.; Blake, A. J.; Wilson, C.; Love, J. B. *Inorg. Chim. Acta* **2007**, *360*, 273.

(10) Givaja, G.; Volpe, M.; Leeland, J. W.; Edwards, M. A.; Young, T. K.; Darby, S. B.; Reid, S. D.; Blake, A. J.; Wilson, C.; Wolowska, J.; McInnes, E. J. L.; Schröder, M.; Love, J. B. *Chem. Eur. J.* **2007**, *13*, 3707.

(11) (a) Cuesta, L.; Tomat, E.; Lynch, V. M.; Sessler, J. L. *Chem. Commun.* **2008**, *32*, 3744. (b) Veauthier, J. M.; Tomat, E.; Lynch, V. M.; Sessler, J. L.; Mirsaidov, U.; Markert, J. T. *Inorg. Chem.* **2005**, *44*, 6736. (c) Sessler, J. L.; Tomat, E.; Mody, T. D.; Lynch, V. M.; Veauthier, J. M.; Mirsaidov, U.; Markert, J. T. *Inorg. Chem.* **2005**, *44*(7), 2125. (d) Sessler, J. L.; Cho, W.-S.; Dudek, S. P.; Hicks, L.; Lynch, V. M.; Huggins, M. T. *J. Porphyrins Phthalocyanines* **2003**, *7*, 97. (e) Veauthier, J. M.; Cho, W.-S.; Lynch, V. M.; Sessler, J. L. *Inorg. Chem.* **2004**, *43*, 1220.

(12) Givaja, G.; Volpe, M.; Edwards, M. A.; Blake, A. J.; Wilson, C.; Schröder, M.; Love, J. B. *Angew. Chem., Int. Ed.* **2007**, *46*, 584.

(13) Chang, C. J.; Loh, Z.-H.; Shi, C.; Anson, F. C.; Nocera, D. G. *J. Am. Chem. Soc.* **2004**, *126*, 10013.

(14) Le Mest, Y.; Inisan, C.; Laouenan, A.; L'Her, M.; Talarmin, J.; El Khalifa, M.; Saillard, J.-Y. *J. Am. Chem. Soc.* **1997**, *119*(26), 6095.

(15) Burger, H.; Wannagat, U. *Monatsh. Chem.* **1963**, *94*, 1007.

dried over appropriate drying agents (K: C_6D_6, d_5-pyridine; activated Al_2O_3: $CDCl_3$), trap-to-trap distilled, and freeze−pump−thaw degassed three times before use. All other solvents and reagents were used as received. ^{1}H NMR spectra were recorded using a Bruker ARX250 spectrometer operating at 250.13 MHz, with residual protic impurities serving as an internal standard. Electrospray mass spectra were recorded using a Thermo-Finnigan LCQ Classic ion trap mass spectrometer. Solutions of $[Co_2(O_2)(L)]$ at concentrations of 18 or 9 μM were prepared in laboratory-grade acetonitrile (purchased from Fischer Scientific and used without further purification) and injected at a flow rate of between 5 and 7 μL/min into the ion trap mass spectrometer via the external, atmospheric pressure electrospray ionization (ESI) source held at a potential of 4.5 kV. The resultant ions were transferred through a heated capillary (63 °C) and focused through two octapole lenses prior to entering the quadrupole ion trap where ions are collisionally cooled with helium buffer gas. UV/vis spectra were recorded on a Perkin-Elmer Lambda 5 spectrophotometer and IR spectra on a Nicolet Avatar 320 FTIR spectrometer equipped with an ATR device or as Nujol mulls. Fluid solution electron paramagnetic resonance (EPR) spectra were recorded at 300 K in THF using a Bruker EPX080 spectrometer and were simulated using the Bruker WINEPR SimFonia program. Magnetic susceptibilities were determined in solution using Evans' method,[16] and the data were corrected for the diamagnetic contribution using Pascal's constants. X-ray photoelectron spectroscopy (XPS) data were recorded by Emily F. Smith of the University of Nottingham on solid samples mounted on adhesive tape using a Kratos AXIS ULTRA X-ray Photoelectron Spectroscopy instrument employing a monochromated Al Kα X-ray source ($h\nu$ = 1486.6 eV) and were processed using the CASA XPS software package (version 2.3.2). Elemental analyses were carried out by Stephen Boyer at the London Metropolitan University.

Synthesis of $[Co_2(L)]$ and $[Co_2(py)_2(L)]$. Under nitrogen, a solution of $[Co(thf)\{N(SiMe_3)_2\}_2]$ (2.30 g, 4.96 mmol) in THF (15 mL) was added dropwise by cannula to a suspension of H_4L (1.50 g, 2.48 mmol) in THF (50 mL) at room temperature. The resulting deep red solution was stirred for 16 h, evaporated to dryness under vacuum conditions, and extracted into hot toluene (50 mL). The hot solution was then filtered by cannula and the filtrate stored at −30° overnight. Deep red crystals of $[Co_2(L)]$ (0.89 g, 50%) were isolated by decanting the supernatant liquors and were dried under vacuum conditions. X-ray-quality crystals of $[Co_2(L)]$ were grown by slow-cooling (−30°) a saturated toluene solution, while diffusion of Et_2O into a toluene/pyridine solution afforded black crystals of the doubly solvated species $[Co_2(py)_2(L)]$.

Analysis for $[Co_2(L)]$ found: C, 63.4; H, 4.43; N, 15.6. $C_{38}H_{32}N_8Co_2$ requires: C, 63.5; H, 4.49; N, 15.6%. ^{1}H NMR (C_6D_6): δ_H 77.4 (br.s, 4H), 39.0 (br.s, 4H), −10.7 (br.s, 4H), −26.1 (br.s, 6H), −30.4 (br.s, 10H), −45.8 (br.s, 4H). Magnetic susceptibility (C_6D_6): μ_{eff} = 3.40 μ_B. UV/vis (THF): λ_{max} 214 (243700), 262 (64117), 270 (57270), 329 nm (ε = 81745 mol^{-1} L cm^{-1}).

Synthesis of $[Co_2(O_2)(py)_2(L)]$. Method 1. A stirred suspension of H_4L (0.200 g, 0.331 mmol) in $CHCl_3$ (15 mL) was treated with a solution of $Co(OAc)_2\cdot 4H_2O$ (0.165 g, 0.662 mmol) in MeOH (ca. 1 mL) under an air atmosphere. The resultant mixture was stirred for 0.5 h at room temperature, after which the solids had dissolved, and was treated with a few drops of NEt_3. The deep brown solution was stirred for 8 h, after which the solvent was removed under vacuum conditions. The crude material was redissolved in MeOH (50 mL) and filtered. Solvent was removed from the filtrate under reduced pressure. The resulting solids were redissolved in minimal $CHCl_3$ and the crude pale brown solids precipitated by the addition of 100 mL of Et_2O and collected by suction filtration (0.188 g, 76%).

Analysis for $[Co_2(O_2)(L)]$ found: C, 60.73; H, 4.41; N, 14.83. $C_{38}H_{32}N_8Co_2O_2$ requires: C, 60.81; H, 4.30; N, 14.93%. IR (ATR): 1613, 1330, 1269, 1204, 1046 cm^{-1}. UV/vis ($CHCl_3$): λ_{max} 324 nm (ε = 29 700 mol^{-1} L cm^{-1}), 480 (6600). ESI-MS: m/z 735 (M^+ + 1). EPR (300K): g 2.028, A(Co) 11.70 G.

The pyridine adduct $[Co_2(O_2)(py)_2(L)]$ was obtained by diffusing Et_2O vapor into a MeOH/pyridine solution of $[Co_2(O_2)(L)]$ as black columns (37%).

UV/vis ($CHCl_3$): λ_{max} 330 nm (ε = 26 100 mol^{-1} L cm^{-1}), 484 (5800). ESI-MS (+ve ion): m/z 735 (M^+ − 2py − O). ^{1}H NMR ($CDCl_3$): δ_H 8.20 (br.s, 4H, *o*/*m*-py), 7.98 (s, 4H, N=C*H*), 7.59 (m, 2H, *p*-py), 7.21 (m, 4H, *o*/*m*-py), 7.12 (d, 4H, J = 3.8 Hz, pyrrole), 6.83 (m, 4H, aryl), 6.38 (br.s, m, 4H, aryl), 6.32 (d, 4H, J = 3.8 Hz, pyrrole), 1.52 (s, 6H, *meso*-CH_3), 1.21 (s, 6H, *meso*-CH_3). EPR (300K, THF): g 2.028, A(Co) 12.04 G, A(N) 2.00 G.

Method 2. A solution of $[Co_2(L)]$ (0.150 g, 0.209 mmol) in dry $CHCl_3$ (25 mL) was degassed and exposed to air, resulting in an immediate dark red to dark brown color change. Pyridine (0.5 mL) was added, and the mixture was reduced in volume. The addition of Et_2O (25 mL) caused 0.085 g, 45%, of $[Co_2(O_2)(py)_2(L)]$ to precipitate as dark brown solids that were isolated by filtration, washed with Et_2O (2 × 5 mL), and dried under vacuum conditions.

Analysis for $[Co_2(O_2)(py)_2(L)]$ found: C, 63.5; H, 4.54; N, 15.3. $C_{48}H_{42}N_{10}Co_2O_2$ requires: C, 63.4; H, 4.62; N, 15.4%.

Synthesis of $[Co_2(OH)(py)_2(L')][Cl]\cdot CH_2Cl_2$. Under air, a solution of $Co(OAc)_2\cdot 4H_2O$ (0.112 g, 0.447 mmol) in MeOH (4 mL) was added to a stirred suspension of H_4L' (0.150 g, 0.213 mmol) in CH_2Cl_2 (15 mL) (H_4L' is an analogue to H_4L that incorporates 2,3-naphthyl aromatic hinge groups derived from 2,3-naphthyldiamine). The resultant mixture was stirred for 20 min at room temperature, during which the solids had dissolved, and was treated with NEt_3 (ca. 0.2 mL). The dark brown solution was stirred at room temperature for 3.5 h and reduced in volume, and 0.149 g, 82%, of crude $[Co_2(O_2)(L')]$ was precipitated by the addition of Et_2O (20 mL). EPR (300 K, CH_2Cl_2): g 2.027, A(Co) 10.31 G, A(N) 8.00 G. ESI-MS (+ve ion): m/z 835 ($[Co_2(OH)(L')]^+$, 100%). Black crystals of $[Co_2(OH)(py)_2(L')][Cl]\cdot CH_2Cl_2$ that were suitable for X-ray diffraction were obtained by diffusion of Et_2O into a CH_2Cl_2/pyridine solution. The chloride likely originated from the contamination of the bench CH_2Cl_2 solvent by HCl. Repeated efforts to obtain microanalytical data were unsuccessful, presumably as both hydroxide $[Co_2(OH)(py)_2(L')][Cl]$ and superoxo cation $[Co_2(O_2)(py)_2(L')]^+$ are present. ^{1}H NMR ($CDCl_3$/CD_3OD): δ_H 7.69 (t, 2 H, J = 7.52 Hz, pyridine), 7.58 (s, 4 H, imine), 7.38 (m, 4 H, pyridine), 7.32 (m, 4 H, aryl), 7.19 (m, 4 H, aryl), 7.12 (t, 4 H, J_{HH} 7.20 Hz, pyridine), 7.08 (s, 4 H, aryl), 7.01 (d, 4 H, J = 4.07 Hz, pyrrole), 6.30 (d, 4 H, J = 4.06 Hz, pyrrole), 1.22 (s, 6 H, CH_3), 1.20 (s, 6 H, CH_3). ESI-MS (+ve ion): m/z 914 ($[Co_2(OH)(py)(L')]^+$, 20%), 835 ($[Co_2(OH)(L')]^+$, 100).

Catalytic Measurements. i. Rotating Ring Disk Electrochemistry. Rotating ring disk (RRD) voltammograms were recorded in aqueous 1.0 M CF_3CO_2H at 10 mVs^{-1} using a conventional three-electrode cell comprising a Pine Instruments E6 series "ChangeDisk" rotating-ring-disk working electrode with a pyrolytic edge-plane-graphite (EPG) disk (area = 0.192 cm^2, Le Carbone, Sussex, UK) and a concentric platinum ring held at +1.0 V versus AgCl/Ag, a platinum wire as the counter electrode, and a AgCl/Ag reference electrode separated from the bulk by a salt bridge. The working electrode was rotated using a Pine Instruments AFMSRCE modulated speed rotator, and experiments were controlled, and data recorded, by a PC-operated AFCBB1 bipotentiostat. Before use, the EPG disk was polished separately from the Pt ring with 600 grit SiC

(16) (a) Schubert, E. M. *J. Chem. Educ.* **1992**, *69*, 62. (b) Evans, D. F. *J. Chem. Soc.* **1959**, 2003.

Chart 2

[Cat], M	[Cp_2Fe^+], M	[H_2O_2], M	k_{obs}, s^{-1}	[H_2O]	% H_2O_2	TON H_2O	TOF H_2O, s^{-1}
1.2E-05	7.4E-04	2.6E-05	0.0079	1.7E-04	14.93	14.5	0.0145
1.2E-05	6.8E-04	7.8E-06	0.0057	1.7E-04	4.72	14.1	0.0141
1.2E-05	8.0E-04	1.3E-05	0.0050	1.9E-04	6.49	16.4	0.0164
1.8E-05	5.7E-04	8.6E-06	0.0084	1.4E-04	6.23	7.82	0.0078
1.8E-05	5.4E-04	8.5E-06	0.0077	1.3E-04	6.50	7.37	0.0074
1.8E-05	5.2E-04	8.5E-06	0.0080	1.3E-04	6.83	7.04	0.0070
2.4E-05	7.5E-04	2.4E-05	0.0056	1.8E-04	13.59	7.34	0.0073
2.4E-05	7.8E-04	1.4E-05	0.0056	1.9E-04	7.38	7.84	0.0078
2.4E-05	6.7E-04	1.2E-05	0.0059	1.6E-04	7.17	6.74	0.0067

paper, sonicated in distilled water for 1 min, and wiped dry. A solution of the catalyst (~0.1 mM) in THF was dropped on the surface of the disk, and the solvent was allowed to evaporate.

ii. Solution Method. The reduction of dioxygen catalyzed by [Co_2(L)] was studied in triplicate for three different catalyst concentrations using a modification of the procedures developed by Fukuzumi and co-workers.[17] In a typical experiment, a solution of [Co_2(L)] (1.2×10^{-5} M) in anhydrous PhCN in the presence of an excess of Cp_2Fe (0.1 M) was transferred into a Teflon-tapped UV−vis quartz cuvette under an inert atmosphere; a second aliquot of the same PhCN was then aerated and used to prepare a standard 0.02 M solution of CF_3CO_2H. A measured aliquot of this solution was then added to the UV cuvette such that the total concentration of O_2 (1.73 mM) was known. As soon as the solution of acid in PhCN was added (mixing was achieved by adding the acid by syringe to the bottom of the cuvette), the measurement was started and the concentration of ferrocenium produced was monitored at 620 nm (ε = 330 M^{-1} cm^{-1}) until asymptotic behavior was observed. At the end of each hour-long experiment, the solution was deaerated to inhibit any further reaction and treated with an excess of NaI. Diluted solutions were analyzed by UV−vis spectrophotometry at 365 nm (ε = 28 000 $M^{-1}cm^{-1}$) to quantify the I_3^- formed and so determine the amount of H_2O_2 present. Background oxidation of ferrocene by O_2 in the presence of acid under the same experimental conditions was subtracted from the data, and the quantity of H_2O_2 (~2×10^{-5} M) was determined by the above iodometric analysis. The function $\ln(A_\infty - A_t)$ was plotted versus time (for the first 100s), and the *pseudo*-first-order rate constant k_{obs} was obtained as the slope of the graph for three different catalyst concentrations. Turnover frequency was calculated on the basis of a 1000 s experiment (see Chart 2).

Calculations. Restricted geometry optimizations were carried out for models of [$Co_2(O_2)(py)_2$(L)] and [$Co_2(O_2)(py)_2$(L)]$^+$ using coordinates derived from the X-ray crystal structure of [$Co_2(O_2)(py)_2$(L)]. The electronic structures of the complexes were constrained to be low-spin during the geometry optimizations, in line with the electronic structures determined from NMR and EPR experiments. The calculations were carried out using the Amsterdam Density Functional (ADF) suite, version 2007.01.[18] The DFT geometry optimizations employed Slater-type orbital triple-ζ-plus polarization basis sets (from the TZP database of the ADF suite) and the frozen core approximation (up to and including 3p for Co and 1s for C, N, and O). The local density approximation with the correlation potential due to Vosko et al.[19] was used in all of the calculations, and gradient corrections were carried out using the functionals of Becke[20] and Perdew.[21] We used the ADF-COSMO (conductor-like screening model) component of the ADF suite to calculate the solvation energies of [$Co_2(O_2)(py)_2$(L)] and [$Co_2(O_2)(py)_2$(L)]$^+$ in dichloromethane solution with a dielectric constant of 8.90 and a radius of the (rigid sphere) solvent molecules of 2.94 Å.[22]

Scheme 1. Formation of Binuclear Cobalt Complexes of the Macrocyclic Ligands L and L′ (Where L′ Is Derived from 2,3-Diaminonaphthalene)

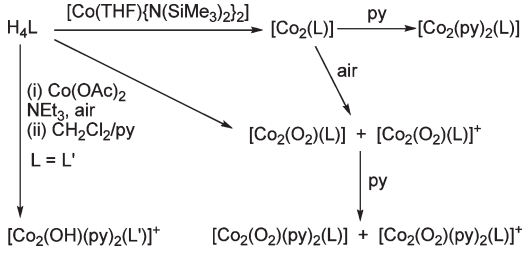

Results and Discussion

Synthesis and Structures of the Binuclear Co(II) Macrocyclic Complexes, [Co_2(L)] and [$Co_2(py)_2$(L)]. The transamination reaction between the macrocycle H_4L and two molar equivalents of the low-coordinate cobalt(II) silylamide, [Co(THF){$N(SiMe_3)_2$}$_2$], resulted in the clean formation of the binuclear complex [Co_2(L)] that was isolated as a dark red microcrystalline solid in good yield (Scheme 1).

The ^{1}H NMR spectrum of this paramagnetic material (μ_{eff} = 3.40 μ_B by Evans' method) shows a series of broad resonances between +78 and −46 ppm that are consistent with a symmetric, wedge-shaped structure in solution, as two sets of *meso*-methyl group protons, assigned by integration, are observed at −26.1 and −30.4 ppm (the latter resonance overlaps coincidently with a 4H resonance). Dark red crystals of [Co_2(L)] suitable for X-ray crystallography were grown from cold toluene, and the solid-state structure is shown in Figure 1, with crystal data and selected bond lengths and angles detailed in Tables 1 and 2, respectively. The addition of pyridine to the crystallization mixture results in the formation of dark red/black crystals of the pyridine adduct [$Co_2(py)_2$(L)], the structure of which was described by us earlier[12] and is shown in Figure 1 for comparison.

[Co_2(L)] crystallizes in the triclinic space group $P\bar{1}$, with two crystallographically independent molecules in the unit cell; reference will be made to only one molecule, as there are no significant differences between these two. As in solution, [Co_2(L)] adopts the wedged, or "Pac-man",

(17) Fukuzumi, S.; Okamoto, K.; Gros, C. P.; Guilard, R. *J. Am. Chem. Soc.* **2004**, *126*(33), 10441.
(18) (a) Fonseca Guerra, C.; Snijders, J. G.; te Velde, G.; Baerends, E. J. *Theor. Chem. Acc.* **1998**, *99*, 391. (b) Velde, G. T.; Bickelhaupt, F. M.; Baerends, E. J.; Guerra, C. F.; Van Gisbergen, S. J. A.; Snijders, J. G.; Ziegler, T. *J. Comput. Chem.* **2001**, *22*, 931.
(19) Vosko, S. H.; Wilk, L.; Nusair, M. *Can. J. Phys.* **1980**, *58*, 1200.
(20) Becke, A. D. *Phys. Rev. A* **1988**, *38*, 3098.
(21) Perdew, J. P. *Phys. Rev. B* **1986**, *33*, 8822.
(22) (a) Klamt, A. *J. Phys. Chem.* **1995**, 2224. (b) Klamt, A.; Jones, V. *J. Chem. Phys.* **1996**, 9972. (c) Klamt, A.; Schüürmann, G. *J. Chem. Soc., Perkin Trans.* **1993**, 799.

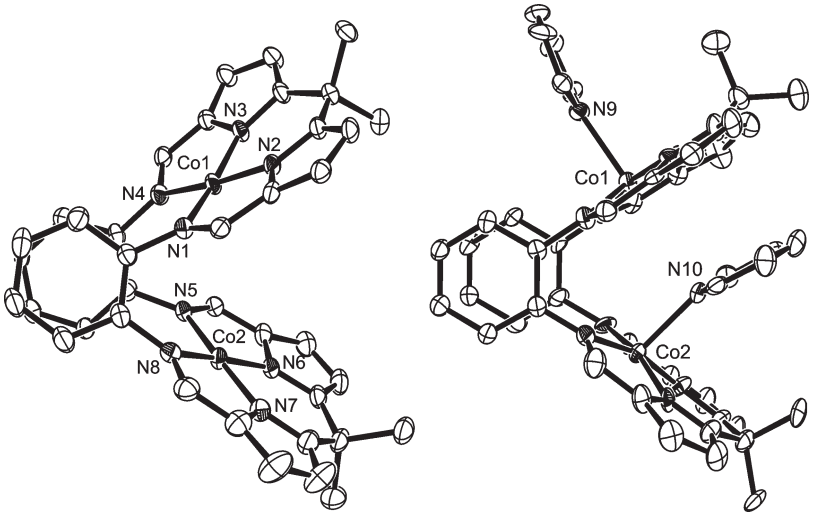

Figure 1. Solid-state structures of $[Co_2(L)]$ (left, one molecule from the asymmetric unit shown) and $[Co_2(py)_2(L)]$ (right) for comparison. For clarity, all hydrogen atoms and solvent molecules have been removed (50% probability displacement ellipsoids).

Table 1. Crystal Data[a]

	$[Co_2(L)]$	$[Co_2(O_2)(MeCN)_2(L)]$	$[Co_2(OH)(py)_2(L)][Cl]$
cryst size [mm]	1.30 × 0.20 × 0.04	0.01 × 0.01 × 0.01	0.30 × 0.18 × 0.15
cryst syst	triclinic	tetragonal	monoclinic
space group	$P\bar{1}$	$I4_1/a$	$P2_1/n$
temp [K]	150 (2)	120 (2)	150 (2)
a, b, c [Å]	12.758(3), 13.278(3), 25.809(5)	13.140(5), 13.140(5), 41.905(9)	12.5220(8), 10.8201(7), 36.754(2)
α, β, γ [deg]	87.028(3), 89.533(3), 68.176(3)	90.00, 90.00, 90.00	90.00, 93.692(1), 90.00
V [Å^3]	4053 (2)	7235 (4)	4969.4 (5)
Z, ρ [mg m^{-3}]	4, 1.404	8, 1.495	4, 1.489
radiation type, λ Å]	Mo Kα, 0.71073	synchrotron, 0.6943	Mo Kα, 0.71073
μ [mm^{-1}]	0.87	0.97	0.88
$2\theta_{max}$ [deg]	55.0	46.28	54.9
diffractometer	Bruker SMART1000 CCD area detector	Bruker SMART APEX2 CCD diffractometer	Bruker SMART APEX CCD area detector
scan mode	ω	fine−slice ω scans	ω
abs correction	multiscan	multiscan	multiscan
T_{min}, T_{max}	0.354, 0.593	0.822, 1.000	0.779, 0.876
measured, independent reflns	35351, 18057	23109, 2604	42508, 11266
structure solution	direct methods using SHELXS	direct methods using SIR-92	direct methods using SHELXS
structure refinement	full-matrix least-squares using SHELXL	full-matrix least-squares using SHELXL	full-matrix least-squares using SHELXL
refinement on	F^2	F^2	F^2
θ_{max} [deg]	27.59	22.68	27.49
No. of params	1011	257	668
H-atom treatment	riding model, rigid rotors for the Me groups	riding model	riding model
$R[F^2 > 2\sigma(F^2)], wR(F^2)$	0.0563, 0.130	0.035, 0.0745	0.0741, 0.1695
$\Delta\rho_{max}, \Delta\rho_{min}$ [e Å^{-3}]	0.97, −0.77	0.48, −0.34	1.944, −0.86
CSD numbers[b]	710017	710018	710019

[a] Computer programs: Bruker SMART version 5.624 (Bruker, 2001); Bruker APEX2; Bruker SMART version 5.625 (Bruker, 2001); SMART (Siemens, 1993); Bruker SAINT version 6.36a (Bruker, 2002); Bruker SAINT; Bruker SAINT version 6.36a (Bruker, 2000); SAINT (Siemens, 1995); Bruker SAINT; Bruker SHELXTL (Bruker, 2001); SHELXS97 (Sheldrick, 1990); Sir-92; SHELXS-97 (Sheldrick, 1990); SIR-92 (Giacovazzo, 1994); SHELXL97 (Sheldrick, 1997); SHELXL-97 (Sheldrick, 1997); ORTEP (Farrugia, 1997); enCIFer (Allen et al., 2004); PLATON (Spek, 2003); enCIFer (Allen et al., 2004). [b] CCDC 710017−710021 contain the supplementary crystallographic data for this paper. These data can be obtained free of charge from the Cambridge Crystallographic Data Centre via www.ccdc.cam.ac.uk/data_request/cif.

conformation in the solid state that has been seen before by us and others for many metal derivatives of this family of ligands. The two metals Co1 and Co2 sit in the center of approximately square-planar N_4-donor environments, in which the sum of the angles at Co1 is 359.95° and at Co2 is 360.13°, with out-of-plane distances of 0.086 and 0.007 Å, respectively. The two metal compartments are not cofacial, as the macrocycle adopts a skewed conformation defined by an average twist angle of 31.3° between the normal to the MN_4 plane and the plane(s) of the aromatic rings; this skewed conformation is further reflected in the Co1···Co2 separation of 4.12 Å. Although the metals sit in an approximately square-planar environment, the *pseudo*porphyrinic cavities are not entirely planar due to the flexibility of the N_4 donor set at the sp^3 hybridized *meso*-carbon; this results in a dihedral angle between the N1−Co1−N2 and N3−Co1−N4 planes of 16.22°, with a smaller value found for the analogous distortion in the Co2 compartment (6.06°). Furthermore, the aromatic "hinges" diverge from

Table 2. Comparison of Key Geometric Parameters from X-Ray and Calculated Data for the Series of Binuclear Cobalt Complexes of L (All Distances (Å) and Angles (deg) Are Averaged unless Singular)[a]

	$[Co_2(L)]$	$[Co_2(py)_2(L)]$, ref 12	$[Co_2(O_2)(py)_2(L)]$, ref 12	$[Co_2(O_2)(py)_2(L)]$ (calculated)	$[Co_2(O_2)(py)_2(L)]^+$ (calculated)	$[Co_2(O_2)(MeCN)_2(L)]$	$[Co_2(OH)(py)_2(L')]^+$
Co−N(pyrrole)	1.847	1.870	1.870	1.898	1.891	1.864	1.863
Co−N(imine)	1.949	1.974	1.984	2.044	2.052	1.998	1.988
Co−N(solv)		2.149	2.071	2.167	2.099	2.126	1.966
Co−O			1.934	1.942	1.891	1.891(7)	1.930
O−O			1.361(3)	1.336	1.334	1.382(14)	
Co···Co	4.12	4.30	4.15	4.12	4.17	3.92	3.61
bite	62.6	64.8	62.7	61.9	62.3	52.9	53.8
twist	31.3	2.9	16.1	15.5	15.8	9.8	5.1
Co−O−O-Co			101.9	101.9	121.0	101.8	
O/N−Co−N(solv)			175.6	173.7	176.0	161.1(2)	179.3

[a] For definitions of bite and twist angles, see ref 10.

coplanarity by 13.2°, although the interplanar distance of 3.438 Å (ring centroid−centroid) suggests the presence of significant π-stacking interactions.

Comparison of the structure of $[Co_2(L)]$ to its doubly solvated analogue (see Table 2 for geometric parameters) shows that both the average Co−N(imino) and Co−N(pyrrole) bond distances are longer in the latter, which is presumably a consequence of the expanded coordination sphere of the metal center. Coordination of pyridine within the cleft also forces the macrocycle to adopt a more symmetric structure in which the twist angle in the pyridine adduct is decreased from 31.3° to 2.9°, the bite angle is increased from 62.6° to 64.8°, and the Co···Co separation is elongated by 0.20 Å. In a similar manner to that seen by us in the binuclear copper complex $[Cu_2(py)(L')]$, where L′ is an analogous macrocycle derived from 2,3-diaminonaphthalene,[10] the pyridine within the cleft adopts an unusually canted geometry in which the aromatic molecule π-stacks to the opposing N_4 plane, with an interplanar distance of 3.44 Å and dihedral angle of 3.3°, and hydrogen-bonds to a suitably oriented *meso*-methyl group ($C_{meso}\cdots pyridine_{centroid}$ = 3.82 Å); this results in a Co2−N10−py $_{centroid}$ angle of 162.3°. This is in contrast to binuclear cofacial diporphyrins that can accommodate solvents such as pyridine in more normal coordination modes within the cleft due to the possibility of considerable vertical expansion,[23] a feature that generally necessitates the use of bulky N-donor ligands such as Bu′-imidazole as axial bases to ensure that no undesired endo-coordination of the solvent occurs. This endo-coordination of small N-donor ligands by single-pillared diporphyrin complexes is exemplified in the X-ray crystal structures of the dicobalt bis(corrole) and the porphyrin−corrole complexes [Co(*exo*-py)Co(*endo*-py)(*exo*-py)(BCA)] and [Co(*exo*-py)(*endo*-py)(H_2PCX)], respectively, where BCA is an anthracyl-bridged bis(corrole) ligand and (H_2PCX) is a xanthyl-bridged porphyrin−corrole ligand in which the porphyrin cavity is unoccupied.[24] In both of these cases, one cobalt center is octahedral, with one of the axial pyridines bound within the binuclear cleft; even so, and unlike in $[Co_2$(*exo*-py)(*endo*-py)(L)], the wide-ranging vertical expansion available to the porphyrinic ligand systems still results in near linear N(py)−Co−N(py) angles.

Synthesis and Structures of Dioxygen Complexes $[Co_2(O_2)(py)_2(L)]$ and $[Co_2(O_2)(MeCN)_2(L)]$. The dioxygen complexes $[Co_2(O_2)(L)]$ and $[Co_2(O_2)(py)_2(L)]$ can be synthesized by two methods: (i) by exposure of $[Co_2(L)]$ to air and (ii) from the aerobic reaction of $Co(OAc)_2$ with H_4L under basic conditions. The former route is more reproducible than the latter, as it avoids problems that sometimes occur due to incomplete deprotonation of the macrocycle that can result in the formation of Co(II) acetate complexes such as $[HNEt_3][\{Co_2(OAc)(\mu\text{-}OAc)(H_2L)\}_2(\mu\text{-}OAc)]\cdot CH_2Cl_2$ (see Supporting Information Figure S1 for X-ray crystal structure). In our previous communication,[12] the X-ray structure of $[Co_2(O_2)(py)_2(L)]$ was described and showed that the dioxygen bridged the two Co centers within the macrocyclic cleft in a zigzag Pauling bonding mode (Figure 2). The O−O bond distance of 1.361(3) Å was found to be between the ranges reported for binuclear cobalt superoxo and peroxo complexes, and furthermore, the Co−N and Co−O bond distances were not indicative of cobalt(II) or cobalt(III) oxidation states. As such, the degree of dioxygen reduction was not easily deduced from the crystallographic data. Instead, the use of ^{1}H NMR, EPR, and in situ magnetic susceptibility experiments allowed us to identify the products of the oxygenation reaction as a mixture of the peroxo complex $[Co_2^{III}(O_2)(py)_2(L)]$ (90%) and the superoxo cation $[Co_2^{III}(O_2)(py)_2(L)]^+$ (10%). The lack of a counterion such as chloride or hydroxide in the above solid-state structure suggests that $[Co_2(O_2)(py)_2(L)]$ is indeed a peroxo-bridged complex. Attempts to oxidize the peroxo complex using standard oxidants such as I_2, either during an EPR experiment or as larger-scale reactions, were unsuccessful. This suggests that the superoxo is not in equilibrium with the peroxo but is instead generated as a result of oxidation of $[Co_2(L)]$ by O_2 to form $[Co_2(L)]^+$, which then reacts rapidly with more O_2 to form $[Co_2^{III}(O_2)(py)_2(L)]^+$. This rationale is consistent with that reported for analogous cofacial diporphyrin systems in which a single-electron reduction of a $[Co_2^{III}(diporph)]^{2+}$ compound is required in order to promote O_2 binding and the formation of the superoxo complex $[Co_2(O_2)(diporph)]^+$.

In an attempt to substantiate further the assignment of the Co oxidation states, XPS data were acquired on solid samples of $[Co_2(L)]$, $[Co_2(py)_2(L)]$, and $[Co_2(O_2)(L)]$. These data display an increase in the Co 2p binding

(23) Deng, Y.; Chang, C. J.; Nocera, D. G. *J. Am. Chem. Soc.* **2000**, *122*, 410.

(24) (a) Barbe, J.-M.; Burdet, F.; Espinosa, E.; Guilard, R. *Eur. J. Inorg. Chem.* **2005**, 1032. (b) Guilard, R.; Jerome, F.; Barbe, J.-M.; Gros, C. P.; Ou, Z.; Shao, J.; Fischer, J.; Weiss, R.; Kadish, K. M. *Inorg. Chem.* **2001**, *40* (19), 4856.

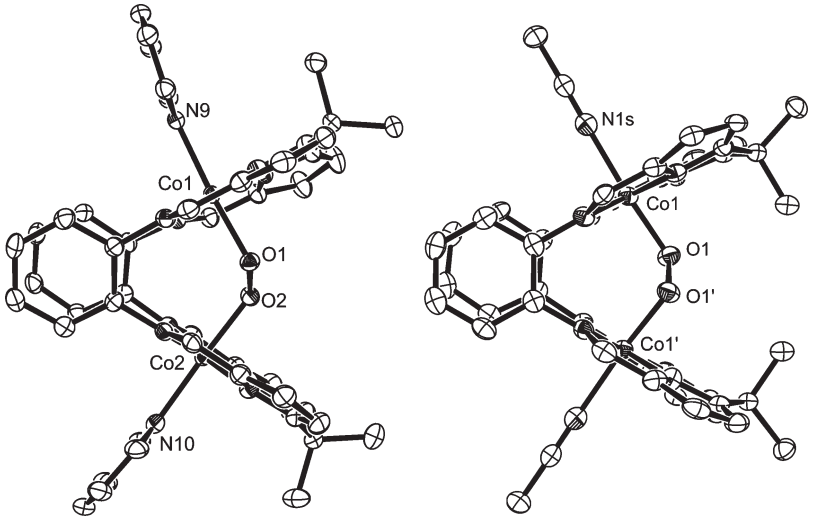

Figure 2. Solid-state structures of the dioxygen complexes $[Co_2(O_2)(py)_2(L)]$ (left)[12] and $[Co_2(O_2)(MeCN)_2(L)]$ (right). For clarity, all hydrogens and solvent of crystallization have been omitted (50% probability displacement ellipsoids). Co1′ and O1′ are the symmetry equivalents of Co1 and O1, respectively.

energy moving from the Co(II) complexes $[Co_2(L)]$ (Co 2p = 777.9 eV) and $[Co_2(py)_2(L)]$ (780.2) to the Co(III) oxygenated compound $[Co_2(O_2)(L)]$ (780.8) that is consistent with an increase in the metal oxidation state. Similarly, XPS studies of Co(salen) complexes and their dioxygen adducts reflect increased binding energies (ca. 1.0 eV) for the Co(III) compounds compared to the Co(II) precursors.[25] For these latter compounds, it was also shown that it is possible to differentiate between superoxo and peroxo through analysis of the O 1s binding energies, which vary by ca. 1.0 eV, but unfortunately, in our case, we were unable to deconvolute the peroxo O 1s peak from background signals.

The sensitive nature of the binuclear complex $[Co_2(L)]$ to aerobic oxidation was highlighted during attempts to crystallize it from cold (−30 °C) MeCN under N_2, which resulted in the formation of dark red prisms. The X-ray crystal structure was determined (Figure 2), and crystal data are detailed in Table 1 and selected bond lengths and angles in Table 2. It is clear from these data that the crystal is a two-component mixture comprising the binuclear cobalt(II) adduct $[Co_2(MeCN)_2(L)]$ and its oxygenated analogue $[Co_2(O_2)(MeCN)_2(L)]$; the data were refined satisfactorily with $wR_1 = 0.0745$ as a disordered merohedral twin with the dioxygen in 42% occupancy. Although the O1−O1′ bond distance of 1.382(14) Å and other Co ligand bond distances are not significantly different from that seen in the pyridine analogue $[Co_2(O_2)(py)_2(L)]$ (Table 2), a small change is seen in the cavity shape with both bite and twist angles, and the Co···Co separation is decreased in the MeCN adduct. It is also clear that the small and rigidly constrained cleft size exhibited by this class of macrocyclic compounds prohibits the linear binding of the MeCN molecule within the cleft, and this contrasts with that seen by us in the binding of the planar pyridine guest in the adducts $[Co_2(py)_2(L)]$ and $[Cu_2(py)(L')]$. Both $[Co_2(O_2)(py)_2(L)]$ and $[Co_2(O_2)(MeCN)_2(L)]$ exhibit extended structures in the solid state that are constructed from intermolecular C−H···O_2 short contacts between the cobalt-bound O_2 and pyridine or acetonitrile solvent CH bonds (see Supporting Information, Figures S2 and S3). In $[Co_2(O_2)(py)_2(L)]$, this results in a zigzag chain of molecules, while molecules of $[Co_2(O_2)(MeCN)_2(L)]$ form a square grid array. This interaction may indicate that the cobalt-bound O_2 possesses some Brønsted basicity, a feature that is desirable for promoting four-electron over two-electron dioxygen reduction chemistry (see below).[13]

Dioxygen Reduction Catalysis. The significance of non-platinum metal catalysts for the reduction of dioxygen led us to evaluate the efficacy of $[Co_2(L)]$ and its oxygenated products that are either generated in situ or as isolated compounds, as catalysts for this process. In the first instance, millimolar solutions of $[Co_2(O_2)(L)]/[Co_2(O_2)(L)]^+$ were generated by dissolution of $[Co_2(L)]$ in aerated CH_2Cl_2 and evaluated by cyclic voltammetry (CV).

The CV of $[Co_2(L)]$ under air between +1.50 and −2.50 V in CH_2Cl_2 displays two irreversible oxidation waves at E_p^a = +0.27 and +0.99 V and an associated weak reduction wave at E_p^c = −0.19 V (Figure 3b). No further reduction waves were seen, except for that due to O_2 reduction by the glassy carbon electrode at E_p^c = −1.30 V (cf. Figure 3a, note: CF_3CO_2H absent). Scanning to high positive potential (> +0.99 V) resulted in the loss of an electrochemical response due to coating of the working electrode. Closer inspection of the CVs between +0.39 and +0.05 V at varying scan rates gave a straight line fit for I_p^a versus $\nu^{0.5}$, consistent with irreversibility of the oxidation at +0.27 V (Supporting Information, Figure S4), and CVs of more reducing voltages displayed related features at E_p^c = +0.10, −0.13, and −0.22 V that are generated only after oxidation to +0.39 V, that is, through an EC mechanism (Figure 3c). Significantly, by comparing the oxidation at +0.27 V to that of ferrocene added to the mixture (3.8 mol equiv, Supporting Information Figure S5), it is clear that the oxidation at +0.27 V for $[Co_2(O_2)(L)]/[Co_2(O_2)(L)]^+$ is for less than one electron. Indeed, controlled potential electrolysis of a 4.6 μM sample of $[Co_2(L)]$

(25) (a) Burness, J. H.; Dillard, J. G.; Taylor, L. T. *J. Am. Chem. Soc.* **1975**, *97*, 6080. (b) Lauher, J. W.; Lester, J. E. *Inorg. Chem.* **1973**, *12*, 244.

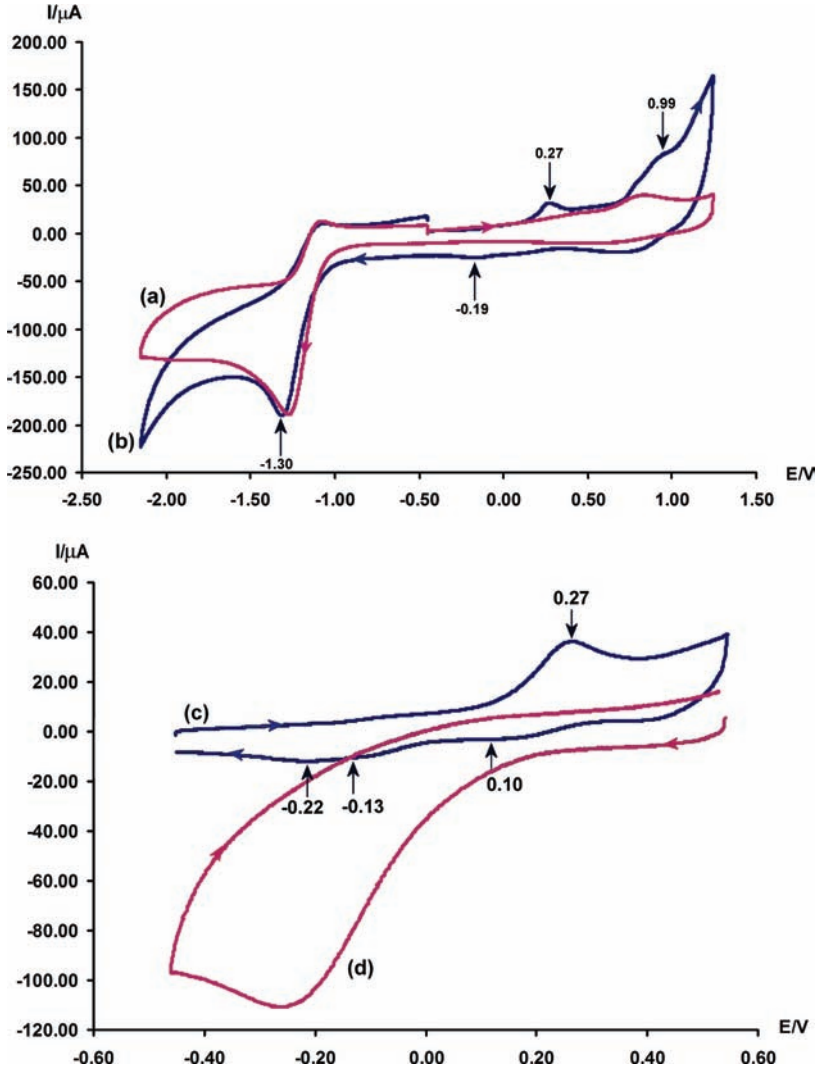

Figure 3. Assessment of $[Co_2(L)]$ as an oxygen reduction catalyst by cyclic voltammetry under air: (a) no catalyst; (b) plus $[Co_2(L)]$; (c) plus $[Co_2(L)]$, range $+0.55$ to -0.45 V; (d) plus CF_3CO_2H. Conditions: 1.0 mM catalyst in CH_2Cl_2, 0.4 M $^nBu_4NBF_4$ versus Fc^+/Fc (AgCl/Ag reference electrode), glassy carbon working electrode (19.6 mm^2), Pt wire counter electrode, scan rate 100 mVs^{-1}.

in the air at $+0.36$ V generated 58 mC of charge, which equates to only 0.13 e^-. However, some insight is gained from these data, as we have shown previously that the reaction of $[Co_2(L)]$ with air generates primarily the peroxo complex $[Co_2(O_2)(L)]$ along with ca. 10% of the superoxo cation $[Co_2(O_2)(L)]^+$. It is therefore likely that the electrochemically active species in this mixture is the latter superoxo cation, with the major peroxo product displaying no redox chemistry, and that the feature at $+0.27$ V represents a one-electron irreversible oxidation to the unstable dication $[Co_2(O_2)(L)]^{2+}$. Furthermore, the lack of any reductive redox processes shows that electrochemical interconversion of the superoxo cation and the peroxo complex does not occur, and so they are presumably formed by different synthetic routes.

The addition of CF_3CO_2H to the electrochemical solution causes the feature at $+0.27$ V to disappear and a large reduction wave with $E_p^c = -0.27$ V to evolve (Figure 3d); this feature is consistent with catalytic dioxygen reduction and occurs at a potential ca. 0.5 V more positive than for glassy carbon alone (note, with no catalyst, $E_p^c = -0.76$ V under the same conditions). No reduction process is observed under a dinitrogen atmosphere. However, under these conditions, this reduction wave is transient as sequential CVs between $+0.55$ and -0.45 V see the height of the E_p^c peak diminish rapidly due to the working electrode becoming coated (Supporting Information Figure S6); repolishing the electrode returns the electrochemical activity briefly before coating reoccurs.

In related cofacial diporphyrin chemistry, Le Mest and co-workers have described the solution electrochemistry of a series of dicobalt cofacial and Pac-man diporphyrin complexes in the presence of O_2.[14] For example, for the Pac-man complex $[Co_2(DPA)]$ (where DPA is an anthracenyl-based single-pillared diporphyrin), they observed two oxidation processes at $E_p^a = 0.00$ V and $E_{1/2} = +0.35$ V (vs Fc^+/Fc) which were assigned to the formation of the hyperoxo complex $[Co_2(O_2)(DPA)]^+$ (i.e., O_2^{3-}), in which the O_2 unit was calculated to be side-on bound, and its single-electron oxidation product $[Co_2(O_2)(DPA)]^{2+}$, respectively; other diporphyrin complexes in this series behaved similarly. The hyperoxo complex $[Co_2(O_2)(DPA)]^+$ was found to react with only 1 equiv of acid to form the new π-radical $[Co_2(O_2H)(DPA)]^{2+}$, which, on the addition of excess acid, resulted in a catalytic reduction wave at the

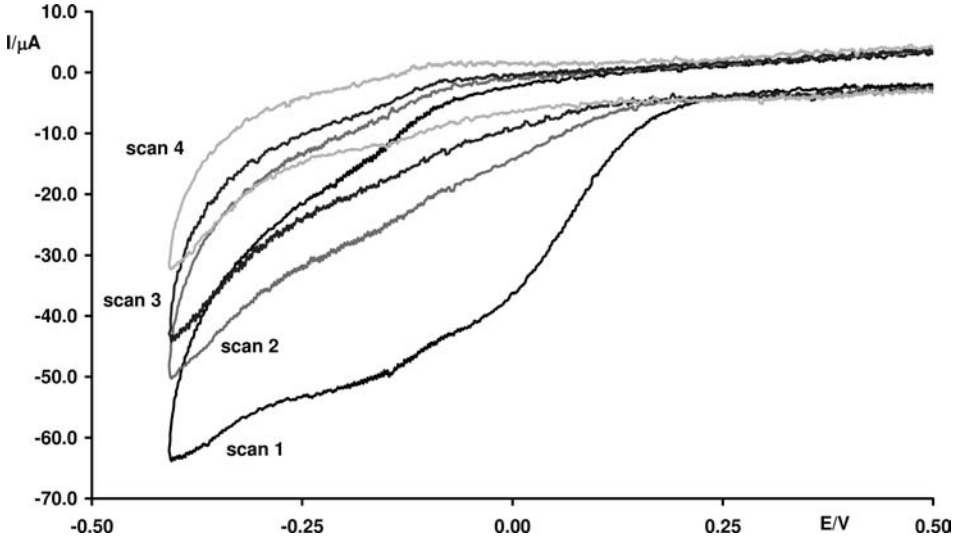

Figure 4. Sequential rotating ring disk electrochemistry of $[Co_2(O_2)(L)]$ adsorbed on an EPG disk in 1.0 M CF_3CO_2H versus AgCl/Ag, rotation rate 500 rpm, Pt ring held at +1.0 V (ring efficiency 23%).

reduction potential of $[Co_2(O_2H)(diporph)]^{2+}$ (ca. 0.0 to −0.12 V). Similar electrochemical observations have been made by Nocera and co-workers for dicobalt complexes of second-generation Pac-man ligands,[6,13] although in this case, the resting state for the catalysis was the $Co^{III}Co^{III}$ superoxo cation $[Co_2(O_2)(diporph)]^+$ in which the O_2 unit was calculated to zigzag between the two metals (i.e., Pauling mode) and was generated by exposure of the cation $[Co^{II}Co^{III}(diporph)]^+$ to air. These observations bear some similarity to those seen by us in the electrochemistry of oxygenated $[Co_2(L)]$. While, in our case, the superoxo complex is formed spontaneously on exposure of $[Co_2(L)]$ to air, the further oxidation and catalytic reduction processes in the presence of acid are seen to occur at potentials similar to those of the cofacial diporphyrin complexes; as such, this suggests that the mechanism of catalytic dioxygen reduction by $[Co_2(L)]$ is similar to that determined for cofacial diporphyrin analogues. In order to assess this reaction further, in particular, to determine the relative proportions of H_2O_2 and H_2O produced, both solid-state and solution electroreduction experiments were carried out.

Rotating ring-disk experiments were carried out using a standard Pine Instruments platinum ring and EPG disk setup.[8,26] Typically, a drop of a $[Co_2(L)]$ solution in THF was allowed to evaporate in the air on the EPG electrode in order to ensure a homogeneous layer of active catalyst. The electrode was then immersed in 1.0 M aqueous CF_3CO_2H, and a preliminary voltammetric scan was recorded between +800 and −800 mV versus Ag^+/Ag. An irreversible reduction wave at about +0.20 V was seen consistently, but as soon as the electrode was rotated, this wave lost intensity to eventually disappear after three voltammetric cycles, preventing the acquisition of a meaningful data set and subsequent Koutecky−Levich analysis (Figure 4).[27] No ring current was detected in any experiments. It is therefore clear that the catalyst either does not adhere to the EPG disk or becomes inactive after a single cycle, as seen in the above CV experiments. Similar effects were observed during RRD electrochemical experiments of binuclear cofacial diporphyrins in which gradual catalyst deactivation occurred and necessitated recoating or complete repolishing and coating of the EPG disk.[28] In this case, it was thought that the catalyst became deactivated through chemical attack by superoxide or peroxide, rather than acid leaching of the chelated metal cation. In order to overcome a possible lack of adherence, attempts were made to graft the catalyst to the surface of the EPG electrode using mixtures of $[Co_2(L)]$ and poly(vinylpyridine), Nafion, or methylcellulose. In each case, a similar reduction wave was observed initially that disappeared while regenerating the electrochemical diffusion layer for a new cycle, which suggests that a redox-inactive complex is being formed during the catalytic cycle.

Fukuzumi and co-workers reported recently a solution method for determining the extent and products of catalytic dioxygen reduction using Cp_2Fe as the electron source in $HClO_4$-acidified, air-saturated benzonitrile.[17] In this method, the oxygen reduction reaction is assessed by monitoring the production of the Cp_2Fe^+ cation at 620 nm by UV−vis spectrophotometry, and from a simple determination of end-point concentration of Cp_2Fe^+, it is possible to identify the number of electrons involved in the process and gain mechanistic insight through rate analysis. By using in situ UV−vis iodometric analysis, the quantity of peroxide can be determined. Using a similar procedure, we have found that $[Co_2(L)]$ catalyzes the PCET reduction reaction between Cp_2Fe, CF_3CO_2H, and O_2 in air-saturated benzonitrile, with the associated generation of a Cp_2Fe^+ cation. The asymptotic behavior of a representative experiment is displayed in Figure 5, plotted as $[Cp_2Fe^+]$ against time, with a representative calculation of k_{obs} inset.

(26) Melin, F.; Boudon, C.; Lo, M.; Schenk, K. J.; Bonin, M.; Ochsenbein, P.; Gross, M.; Weiss, J. *J. Porphyrins Phthalocyanines* **2007**, *11*(3−4), 212.

(27) (a) Chen, J.; Zhang, W.; Officer, D.; Swiegers, G. F.; Wallace, G. G. *Chem. Commun.* **2007**, 3353. (b) Treimer, S.; Tang, A.; Johnson, D. C. *Electroanalysis* **2002**, *14*, 165.

(28) Collman, J. P.; Denisevich, P.; Konai, Y.; Marrocco, M.; Koval, C.; Anson, F. C. *J. Am. Chem. Soc.* **1980**, *102*, 6027.

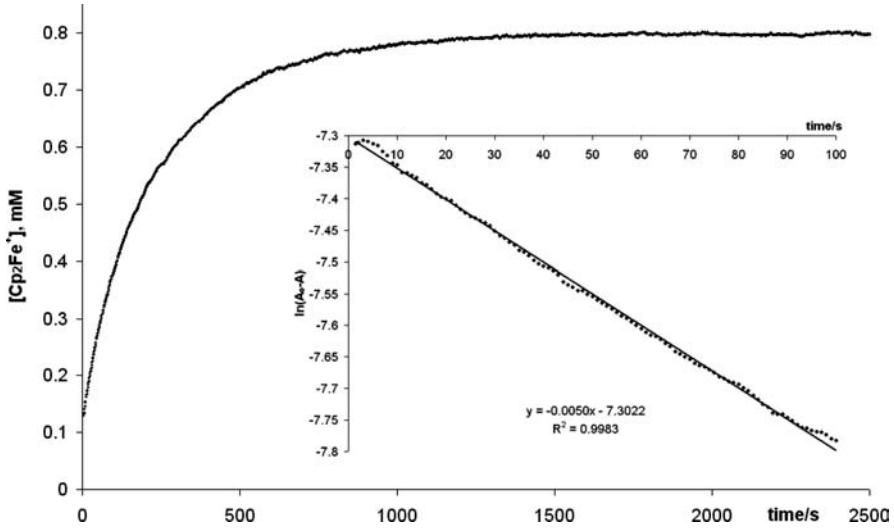

Figure 5. Typical experiment showing the evolution of $[Cp_2Fe]^+$ against time monitored by UV−vis spectrophotometry at 620 nm, catalyst concentration = 1.2×10^{-5} M, initial $[Cp_2Fe]$ = 0.1 M, initial $[CF_3CO_2H]$ = 0.02 M. Inset: calculation of k_{obs} as slope of the plot of $\ln(A_\infty - A_t)$ vs time.

While it is clear from the ratio of end-point concentration of Cp_2Fe^+ versus catalyst concentration (ca. 70:1) that the reaction is catalytic, not all of the dioxygen is consumed; the ratio of $[Cp_2Fe^+]$ to $[O_2]$ is ca. 0.4 and should be 2.0 for H_2O_2 production or 4.0 for H_2O production. As such, we are not able to determine the dioxygen reduction products from the concentration of Cp_2Fe^+. However, in situ analysis of the end-point concentration of peroxide by the addition of iodide to the reaction mixture and subsequent UV−visible spectroscopic determination of I_3^- provides some insight into the peroxide-to-water product ratio. The observed concentration of peroxide of between 7.8×10^{-6} and 2.4×10^{-5} M equates approximately to that determined from the background reaction between O_2, Cp_2Fe, and CF_3CO_2H (2×10^{-5} M after 1 h; see Supporting Information, Figure S7). This suggests that little or no peroxide is formed during the cobalt-catalyzed reaction and that, therefore, in a similar manner to some of the porphyrinic analogues, the four-electron reduction of O_2 to water is the predominant process. Even so, it is clear that in our case the catalytically active component diminishes over time, as only 7−16 turnovers are achieved before the loss of activity. Furthermore, the rate of catalysis is very slow compared to that of the cofacial diporphyrin analogues. Extrapolated values for the pseudo-first-order rate constant k_{obs} average to $3.8(2) \times 10^{-3}$ s^{-1} and are about 3 orders of magnitude smaller than the corresponding values obtained by Fukuzumi and co-workers using cofacial diporphyrins.[17] In these latter cases, the reactions become asymptotic within minutes, while 30−60 min catalytic experiments are required in the case of $[Co_2(L)]$.

Previous experimental and theoretical studies on related Co Pac-man−diporphyrin complexes have found that the formation of a Co^{III}/Co^{III} superoxo species from the reaction between a Co^{III}/Co^{II} cation and O_2 is a critical entry point into the catalytic O_2 reduction cycle.[13,14,29] Superoxo species have also been identified as a key component on platinum surfaces during oxygen reduction catalysis.[30] Also, in the porphyrinic systems, it has been determined that the basicity of the superoxo (or, alternatively, the hyperoxo)[14] complex dictates the mode of catalysis, in that initial protonation of the superoxo complex promotes a four-electron reduction pathway to water, whereas rapid electron transfer first generates a transient peroxo complex which results in the two-electron route being preferred.[13] In our case, we can best consider that the *minor* (10%) superoxo component of the Co material added represents the resting state of the catalytic cycle and that the peroxo compound (90%) is effectively inert; this supposition would result in a 10-fold increase in TON. We noted above that we have been unable to isolate cleanly the superoxo compound $[Co_2(O_2)(L)]^+$, either chemically or electrochemically, and that the peroxo and superoxo compounds are generated by different pathways. It is therefore feasible that the concentration of the catalytically active species decreases during the reaction as diminishing amounts of superoxo complex are formed during the catalytic cycle, as either more peroxo compounds or other inert compounds such as bridged hydroxides are produced (see below).

Mass Spectrometry. Electrospray ionization mass spectrometry and collision-induced dissociation (CID) studies were used to explore the structure and fragmentation pathways of $[Co_2(O_2)(L)]/[Co_2(O_2)(L)]^+$ in the gas phase. In previous electrospray ionization studies on these complexes, we had not been able to stabilize the dioxygen compound, and instead the monoprotonated, single-oxygen-containing species $[Co_2(O)(L)]H^+$ at m/z 735 that results from a loss of O dominated the resulting mass spectrum.[12] In this study, by using an ion-transfer tube temperature (the tube between atmospheric pressure and vacuum) of 63 °C, a temperature considerably lower than is commonly applied in electrospray, the precursor ion $[Co_2(\mu\text{-}O_2)(L)]H^+$ at m/z 751 was successfully detected and stabilized for the first time (Figure 6). Another ion at m/z 768 was also observed and is consistent with the

(29) (a) Collman, J. P.; Hutchison, J. E.; Angel Lopez, M.; Tabard, A.; Guilard, R.; Seok, W. K.; Ibers, J. A.; L'Her, M. *J. Am. Chem. Soc.* **1992**, *114*, 9869. (b) Chang, C. K. *J. Chem. Soc., Chem. Commun.* **1977**, 800. (c) Proniewicz, L. M.; Odo, J.; Goral, J.; Chang, C. K.; Nakamoto, K. *J. Am. Chem. Soc.* **1989**, *111*, 2105.

(30) Shao, M.-H.; Liu, P.; Adzic, R. R. *J. Am. Chem. Soc.* **2006**, *128*, 7408.

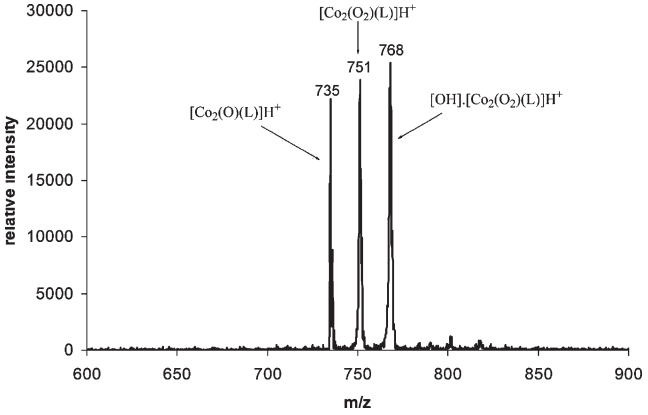

Figure 6. Typical ESI mass spectrum of $[Co_2(O_2)L]H^+$ obtained from an 18 μM solution at low ion transfer capillary temperature (63 °C).

presence of the hydroxyl adduct $[OH]\cdot[Co_2(\mu\text{-}O_2)(L)]H^+$. Significantly, when the ion-transfer tube temperature was increased, the single O-atom bridged species $[Co_2(O)(L)]H^+$ dominated the resulting mass spectrum, reflecting the labile nature of both $[Co_2(\mu\text{-}O_2)(L)]H^+$ and its hydroxyl adduct $[OH]\cdot[Co_2(\mu\text{-}O_2)(L)]H^+$.

In order to further investigate the stability and fragmentation pathways of $[Co_2(O_2)(L)]H^+$ and its monooxygenated analogue $[Co_2(O)(L)]H^+$, CID studies were undertaken. CID is a popular tandem mass spectrometry method by which a particular ion type is activated through collisions with a buffer gas, in this case, helium.[31] The detected products are a result of dissociation pathways including neutral ligand loss and hetero- and homolytic bond cleavage, as well as the possibility of charge-transfer processes for multiply charged ions. The quadrupole ion-trap mass spectrometer used in this study enables the selective trapping and collisional-cooling of a mass-selected ion to produce a mass-normalized collision energy (NCE).[32] As such, by recording CID spectra at increasing NCE, the extent of the activation of fragmentation pathways can be observed and used as a comparison of the relative stabilities of $[Co_2(O)(L)]H^+$ and $[Co_2(O_2)(L)]H^+$ in the gas phase (Figure 7). It can be seen that higher collision energies are required to activate the fragmentation pathways of the single O-atom-bridged ion, $[Co_2(O)(L)]H^+$. Notably, for $[Co_2(O_2)(L)]H^+$, the most facile loss is of a single oxygen atom, while in the case of the monooxygenated species, a loss of a CH_3 groups from the macrocyclic ligand is preferred. Indeed, we were not able to stabilize the deoxygenated ion $[Co_2(L)]$ in this series of CID experiments, which suggests that the single O-atom bridged motif is particularly stable.

Isolation and Structural Characterization of Single O-Atom Bridged Complexes. Using a similar method to generate the dioxygen complex $[Co_2(O_2)(py)_2(L)]$, the aerobic reaction between $Co(OAc)_2$ and H_4L' under basic conditions (H_4L' is an analogue to H_4L that incorporates 2,3-naphthyl aromatic hinge groups derived from 2,3-diaminonaphthalene) results in the formation of the new dicobalt complex $[Co_2(\mu\text{-}OH)(py)_2(L')][Cl]$ after recrystallization from bench CH_2Cl_2/Et_2O in the presence of pyridine. Analysis of the crude mixture by EPR spectroscopy revealed a very weak 15-line spectrum at $g = 2.027$ due to the presence of the superoxo cation $[Co_2(O_2)(L')]^+$, so it is probable that this dioxygen complex has formed initially but is relatively unstable compared to the isolated hydroxy-bridged complex. The ^{1}H NMR spectrum of the crude mixture reveals resonances consistent with diamagnetic $[Co_2(\mu\text{-}OH)(py)_2(L')][Cl]$ and so supports the assignment of Co(III) oxidation states, and the presence of two resonances for the *meso*-methyl protons at 1.22 and 1.20 ppm implies that a wedged geometry is adopted in solution. Black crystals of $[Co_2(\mu\text{-}OH)(py)_2(L')][Cl]$ were obtained by the diffusion of Et_2O into a mixture of CH_2Cl_2 and pyridine, and the solid-state structure is shown in Figure 8, with crystal data and selected bond lengths and angles detailed in Tables 1 and 2, respectively.

The complex $[Co_2(\mu\text{-}OH)(py)_2(L')][Cl]$ crystallizes as a CH_2Cl_2 solvate in the monoclinic system, space group $P2_1/n$, and reveals the presence of a bridging oxygen atom within the cleft and a chloride counterion. The dichloromethane solvent of crystallization contains a disordered chlorine atom Cl1 that was modeled over two sites with ca. 70:30 occupancy. The two Co atoms Co1 and Co2 sit in octahedral environments defined by the two imino and two pyrrolic nitrogens, apical pyridines and the bridging oxygen atom. Even though the hydrogen was not located from the difference Fourier map, the latter oxygen is best defined as a bridging hydroxyl group rather than an oxo group due to a combination of the presence of the chloride counterion and the diamagnetism of the complex. This is further substantiated by the average Co−O1 bond distance of 1.930 Å, which is similar to other six-coordinate Co(III) bridging hydroxide complexes (mean 1.917 ± 0.036 Å).[33] The bridging hydroxide sits within the cleft of the macrocycle with a Co1−O1−Co2 angle of 138.4° that is considerably more obtuse than in reported examples (mean 102.0 ± 8.7°)[33] and is presumably a consequence of the very rigid environment provided by the macrocycle. The presence of the hydroxyl bridge causes the bite angle of the Pac-man wedge to decrease to 53.8° and limits the degree of torsional twisting in the solid state to 5.1°, which results in a Co···Co separation toward the lower limit of this series of compounds.

A second hydroxy-bridged dicobalt complex $[Co_2(OH)(Me_2Im)(HL)](MeCN)_4(H_2O)$ crystallized in small quantities from acetonitrile during attempts to isolate $[Co_2(L)]$ in the presence of 1,2-dimethylimidazole (Me_2Im). The X-ray structure of this molecule (Supporting Information, Figure S8) showed that hydrolysis of a Co−N(pyrrole) bond had occurred, to result in a $Co^{II}(\mu\text{-}OH)Co^{II}$ motif in which one of the two five-coordinate Co cations has migrated around the macrocycle to span the aryldiamine nitrogens. A similar bonding arrangement for the Co(II) cations is seen in $[HNEt_3][\{Co_2(OAc)(\mu\text{-}OAc)(H_2L)\}_2(\mu\text{-}OAc)]$ (see Supporting Information, Figure S1), although in contrast two pyrrole nitrogens remain protonated in this latter case. The Co−N and Co−O bond distances in $[Co_2(OH)(Me_2Im)_2(HL)]$ suggest that Co(II) cations are present, as these distances are appreciably longer that those in the Co(III) complex

(31) March, R. E.; Todd, J. F. J. *Quadrupole Ion Trap Mass Spectrometry*, 2nd ed.; Wiley Interscience: New York, 2005; p 120.

(32) Thermo-Scientific Normalised Collision Energy Technology; Product Support Bulletin 4. www.thermo.com/ms (accessed Apr 2009).

(33) Fletcher, D. A.; McMeeking, R. F.; Parkin, D. *J. Chem. Inf. Comput. Sci.* **1996**, *36*, 746.

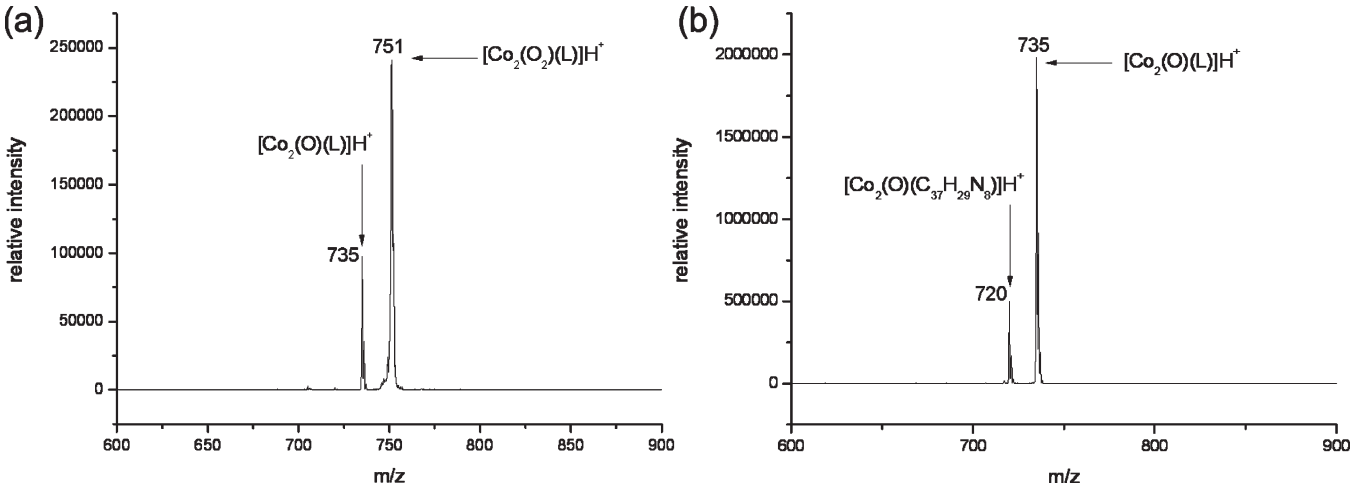

Figure 7. Collision-induced dissociation spectra recorded for the precursor ions (a) $[Co_2(O_2)(L)]H^+$ at 7% NCE and (b) $[Co_2(O)(L)]H^+$ at 24% NCE.

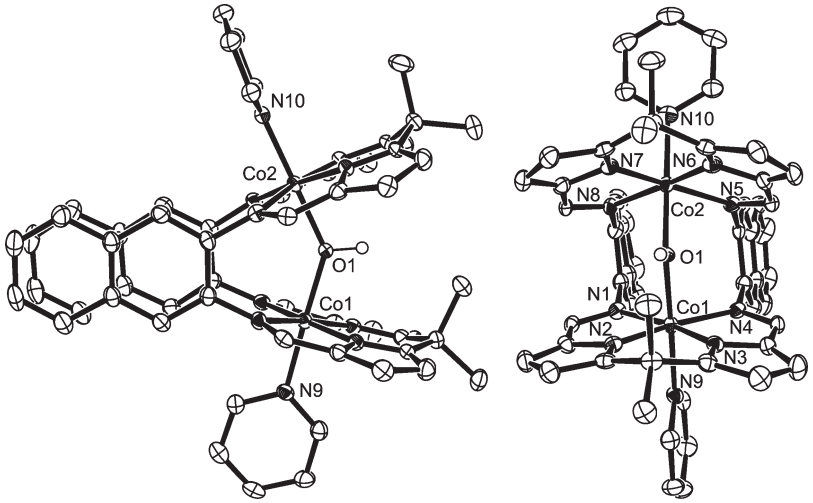

Figure 8. Side-on and face-on views of the solid-state structure of $[Co_2(OH)(py)_2(L')][Cl]\cdot CH_2Cl_2$. For clarity, all hydrogen atoms except that on O1, the chloride anion, and the solvent of crystallization have been omitted (50% probability displacement ellipsoids).

$[Co_2(OH)(py)_2(L')]^+$. This is corroborated by comparison to $[Co_2(\mu\text{-OH})(taec)][ClO_4]_3$ (taec = aminoethyl-substituted tetraazacyclotetradecane), a rare example of a structurally characterized, singly hydroxide-bridged binuclear Co(II) complex.[34]

Calculations. The structural data from Amsterdam Density Functional calculations for $[Co_2(O_2)(py)_2(L)]$ and $[Co_2(O_2)(py)_2(L)]^+$ and those derived from X-ray crystallographic studies are compared in Table 2. The calculated structure of $[Co_2(O_2)(py)_2(L)]$ reproduces the principal features of the structure of $[Co_2(O_2)(py)_2(L)]$ determined by X-ray crystallography, including the zigzag $\kappa^1{:}\kappa^1$ Pauling bonding mode within the $[Co_2(O_2)]^{4+}$ unit and the bite and twist angles (bite = 61.9° and twist = 15.5°) between the macrocylic components. The calculated metal−ligand distances are within 0.060 Å of the experimental values, except for those involving the coordinated pyridine ligands which are ca. 0.096 Å longer in the calculated structure. Thus, it is likely that the calculations reproduce qualitatively the principal features of the electronic structure of $[Co_2(O_2)(py)_2(L)]$. We also carried out calculations on $[Co_2(O_2)(py)_2(L)]^+$ since no experimental structure is available for this complex and because this species had been identified as a minor product (ca. 10%) in the reaction of $[Co_2(L)]$ with O_2. The superoxo complex $[Co_2(O_2)(py)_2(L)]^+$ possesses a similar electronic structure to that of peroxo $[Co_2(O_2)(py)_2(L)]$, in which the composition of the semioccupied molecular orbital (SOMO) of $[Co_2(O_2)(py)_2(L)]^+$ (Figure 9b) is essentially identical to that of $[Co_2(O_2)(py)_2(L)]$ and is derived from the removal of one electron from the highest occupied molecular orbital (HOMO) of $[Co_2(O_2)(py)_2(L)]$ (Figure 9a). The compositions of the SOMO in $[Co_2(O_2)(py)_2(L)]^+$ and HOMO in $[Co_2(O_2)(py)_2(L)]$ are 40.2% O 2p and 32.1% Co 3d and 39.6% O 2p and 45.0% Co 3d, respectively.

The calculated structure of $[Co_2(O_2)(py)_2(L)]^+$ retains the principal features of the coordination spheres about each metal found in $[Co_2(O_2)(py)_2(L)]$, with no significant variation in the Co−N (pyrrole and imine) and Co−O distances. $[Co_2(O_2)(py)_2(L)]^+$ possesses similar bite and twist angles (bite = 62.3° and twist = 15.8°) to those found for the calculated structure of $[Co_2(O_2)(py)_2(L)]$ (Table 2). The principal differences in geometry between $[Co_2(O_2)(py)_2(L)]$ and $[Co_2(O_2)(py)_2(L)]^+$ lie within the

(34) Mikuriya, M.; Kida, S.; Kohzuma, T.; Murase, I. *Bull. Chem. Soc. Jpn.* **1988**, *61*, 2666.

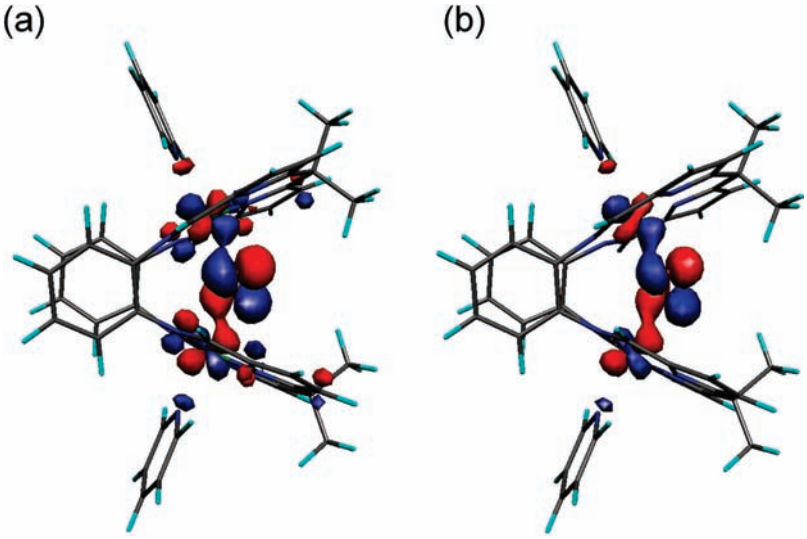

Figure 9. The Kohn−Sham representations of (a) the HOMO in $[Co_2(O_2)(py)_2(L)]$ and (b) the SOMO of $[Co_2(O_2)(py)_2(L)]^+$ at the 0.04 e Å^{-3} isosurface. (The program MOLEKEL[35] was used to prepare the three-dimensional plots of the electron density.)

$[Co_2(py)_2(O_2)]^{3+}$ unit. For $[Co_2(O_2)(py)_2(L)]^+$, the Co−N(py) and Co−O distances shorten by 0.094 and 0.043 Å, respectively, and the Co−O−O−Co dihedral angle increases from 101.9° in $[Co_2(O_2)(py)_2(L)]$ to 121.0° in $[Co_2(O_2)(py)_2(L)]^+$. Significantly, however, the O−O distance is effectively unchanged on oxidation, decreasing very slightly from 1.336 Å in $[Co_2(O_2)(py)_2(L)]$ to 1.334 Å in $[Co_2(O_2)(py)_2(L)]^+$, and suggests that this bond distance is not a good measure of the formal electronic structure of these macrocyclic complexes and that the macrocyclic framework acts as a geometric constraint. In order to gain insight into the relative stabilities of the $[Co_2(O_2)(py)_2(L)]$ and $[Co_2(O_2)(py)_2(L)]^+$ complexes, we computed the reduction potential of the $[Co_2(O_2)(py)_2(L)]^{+/0}$ couple in CH_2Cl_2 solution and evaluated the molecular energies for the oxidized and reduced species in the same solvent:[36]

$$V = -[(E_{red} - E_{ox}) + (\Delta G_{red}^{CH_2Cl_2} - \Delta G_{ox}^{CH_2Cl_2})] - V_0$$

where E_x and $\Delta G_x^{CH_2Cl_2}$ are the theoretical molecular and solvation energies, respectively, and V_0 is the absolute potential (4.43 V)[37] of the normal hydrogen electrode (NHE). Using this methodology, we calculated a reduction potential of +0.37 V versus NHE for the $[Co_2(O_2)(py)_2(L)]^{+/0}$ couple (−0.18 V vs Fc^+/Fc); as such, the calculations suggest that the peroxo species $[Co_2(O_2)(py)_2(L)]$ is more thermodynamically stable than the superoxo cation $[Co_2(O_2)(py)_2(L)]^+$ in dichloromethane solution. This potential, together with the lack of electrochemical interconversion seen above between the peroxo and superoxo complexes, and the possible formation of very stable hydroxy-bridged motifs to form compounds such as $[Co_2(\mu\text{-}OH)(L')]^+$, may inhibit access to the catalytically relevant superoxo $[Co_2(O_2)(py)_2(L)]^+$ complex and depress the activity of these complexes toward oxygen reduction catalysis.

(35) Portmann, S.; Luthi, H. P. *Chimia* **2000**, *54*, 766.
(36) Fu, Y.; Liu, L.; Yu, H.-Z.; Wang, Y.-M.; Guo, Q.-X. *J. Am. Chem. Soc.* **2005**, *127*, 7227.
(37) Reiss, H.; Heller, A. *J. Phys. Chem.* **1985**, *89*, 4207.

Conclusions

We have shown that a variety of di-cobalt Pac-man complexes of straightforwardly synthesized Schiff-base calixpyrrole ligands can be prepared, and that their structures and chemistry related to oxygen reduction display some similarity to those of cofacial diporphyrins. The dicobalt complex $[Co_2(L)]$ reacts readily with O_2 to form not only the peroxo complex $[Co_2(O_2)(L)]$ but also the superoxo cation $[Co_2(O_2)(L)]^+$ as a minor component. This mixture acts as a catalyst for the reduction of oxygen to water, albeit at a low turnover number and frequency. As with the related cofacial diporphyrin chemistry, our present understanding based on electrochemical, mass spectrometric, catalytic, and DFT experiments is that the superoxo cation $[Co_2(O_2)(L)]^+$ is the catalytically relevant species yet is disfavored when compared to peroxo $[Co_2(O_2)(L)]$ and hydroxy-bridged species $[Co_2(OH)(L)]^+$. It is therefore clear that while this bimetallic structural motif can manage the proton and electron inventories necessary to carry out this reduction chemistry, modifications are required to inhibit the formation of peroxo and single-atom bridged complexes and to promote the formation of the superoxo cation $[Co_2(O_2)(L)]^+$.

Acknowledgment. We thank the Universities of Edinburgh and Nottingham for their support, the British Mass Spectrometry Society and the Nuffield Foundation for their provision of undergraduate research bursaries to K.W. and H.H., respectively, Prof. Bill Clegg of the University of Newcastle and the EPSRC X-Ray Diffraction Service at the University of Southampton for the collection of X-ray data at the Synchrotron Radiation Source, Daresbury, and Dr. E. Stephen Davies at the University of Nottingham for assistance with some of the cyclic voltammetry experiments.

Supporting Information Available: Additional figures and tables. This material is available free of charge via the Internet at http://pubs.acs.org.